EARTHQUAKE ENGINEERING AND STRUCTURAL DYNAMICS, VOL. 26, 1041–1057 (1997)

A SIMPLIFIED INPUT OUTPUT RELATION METHOD USING AR MODEL FOR EARTHQUAKE WAVE PROPAGATION ANALYSIS

HIDEJI KAWAKAMI*† AND PAUL DE JESUS BIDON‡
Department of Civil Engineering, Saitama University, 255 Shimo-Okubo, Urawa-shi, Saitama 338, Japan

SUMMARY

This paper introduces a Simplified Input Output Relation Method (SIORM) using multiple-variable autoregression (AR) model which can be used to determine ground wave propagation properties. Using the AR model, a method is developed to establish the basis for the formulation of SIORM. The degree of accuracy of this method is evaluated. SIORM is applied to actual ground acceleration records taken at Minamisuna and Etchujima sites in Japan and its results are discussed in this paper. © 1997 John Wiley & Sons, Ltd.

Earthquake Engng. Struct. Dyn., **26**, 1041–1057 (1997)

No. of Figures: 10. No. of Tables: 2. No. of References: 20.

KEY WORDS: wave propagation; autoregression model; time series; impulse

INTRODUCTION

In the past earthquakes, it has been noted that the degree of damage varies from sites. One reason for this is the difference in the soil type of the site. Moreover, a large earthquake magnitude is not necessarily translated into a violent ground movement; much depend on the local geology. An area on top of unstable sand or clay is likely to be shaken up much more than anywhere at the same distance from the epicentre but sitting on granite. A careful study about the influence of soil type on the ground wave propagation properties will greatly help the earthquake engineers mitigate the earthquake destruction.

The ground wave propagation properties can be estimated based on the geophysical exploration[1] and laboratory experiments of boring samples. However, the properties estimated by these methods are rather different from those during strong earthquake motions which are much more complicated. The properties estimated based on analysis of wave forms recorded during earthquakes seem most reliable, and the relationship between waves at different points should be examined.[2–4] These points compose the surface seismic arrays or downhole seismic arrays, and a number of investigations have been conducted based on the transfer function[5–9] of the surface layer in the frequency domain. However, the main objective of these studies is to find the soil property, such as S-wave velocity of each layer, under an assumption of a certain physical soil model, e.g. horizontal layering, and is not to show directly how the wave propagates in the surface layer during the earthquake.

Meanwhile, the time history records in the surface seismic arrays or downhole seismic arrays have also been used to estimate the wave propagation properties, such as the propagation direction, velocity, amplitude, reflection and refraction of waves, by comparing the wave forms directly and by using

* Correspondence to: H. Kawakami, Department of Civil and Environmental Engineering, Saitama University, 255 Shimo-Okubo, Urawa-shi, Saitama 338, Japan
† Professor
‡ Masteral Student

CCC 0098–8847/97/101041–17$17·50

Received 24 September 1996
Revised 10 April 1997

cross-correlation functions[10,11] and F-K spectrum.[12,13] Among these methods, the most common method has been the use of peak of the cross-correlation function. However, there has been a disadvantage in using the said method because the shape of the cross-correlation function is not only greatly influenced by the wave propagation properties but also by the shape of the autocorrelation function. A simple but reliable method should be developed to obtain the wave propagation properties from actual ground acceleration time history records during the earthquake.

In this study, a Simplified Input Output Relation Method (SIORM) which can be used to obtain the ground wave propagation properties is presented. In this method, in order to obtain the relationship between observation points, multiple-variable autoregression (AR) model is used. The discussion of the SIORM is divided into two parts. The first part discusses the method of analysis and evaluation of the accuracy of the method. The second part relates to the application of the method to actual ground acceleration time history records.

METHOD OF ANALYSIS

The method of analysis presented in this paper can be divided into two stages. First, the ground acceleration time series of k different observation points are considered and expressed using autoregression (AR) model.[14–18] In order to express the time series in AR model, coefficient $a_{Mij}(m)$ is computed. After computing the coefficient $a_{Mij}(m)$, the corresponding time series at one observation point can be computed when a time series like a shape of a unit impulse at a particular time has been observed at the other observation point. With the result of the impulse response, the wave propagation properties can be determined.

Determination of coefficient $a_{Mij}(m)$[14]

The stationary time series in k dimension, $\{X(s)\} = \{x_1(s)x_2(s) \ \dots \ x_k(s)\}^{\mathrm{T}}$ $(s = 1, 2, \dots, N)$ (T denotes transposed vector or matrix), are expressed in AR model as

$$\{X(s)\} = \sum_{m=1}^{M} [A_M(m)]\{X(s-m)\} + \{U(s)\} \tag{1}$$

where $\{U(s)\} = \{\varepsilon_1(s)\,\varepsilon_2(s) \ \dots \ \varepsilon_k(s)\}^{\mathrm{T}}$. The vector $\{U(s)\}$ is a k dimensional white noise with mean value of zero. Its cross-correlation is expressed by the formula

$$R_{\varepsilon_i\varepsilon_j}(\iota) = E[\varepsilon_i(s+\iota)\varepsilon_j(s)] = \delta_{\iota 0}\sigma_{ij} \tag{2}$$

where $E[\ ]$ represents the expected value, and the Kronecker delta, $\delta_{\iota 0}$, is defined as

$$\delta_{\iota 0} = \begin{cases} 1 & (\iota = 0) \\ 0 & (\iota \neq 0) \end{cases} \tag{3}$$

Expressing equation (1) in terms of components, it can be expressed as

$$x_i(s) = \sum_{m=1}^{M} \sum_{j=1}^{k} a_{Mij}(m)x_j(s-m) + \varepsilon_i(s) \tag{4}$$

where $i = 1, 2, \dots, k$, $s = 1, 2, \dots, N$ and $a_{Mij}(m) =$ the (i,j) element of $[A_M(m)]$.

The vector $\{X(s)\}$ in equation (1) or equation (4) is expressed by using $\{X(s-1)\}$, $\{X(s-2)\}$, $\dots$, $\{X(s-M)\}$ which are the vectors from time $s-1$ to time $s-M$. For this reason, it is called M order AR model.

In equations (1) and (4), when the number of observation points is k, k multivariable AR model is considered. Coefficient $a_{Mij}(m)$ is computed so that the mean square value of the error $\varepsilon_i(s)$ is minimized. The

autocorrelation or cross-correlation of $x_i(s)$, $x_j(s)$, which is expressed by

$$R_{ij}(\iota) = E[x_i(s+\iota)x_j(s)], \quad (i,j = 1,2,\ldots,k;\ \iota = 1,2,\ldots,M) \tag{5a}$$

and the following equations

$$\sum_{m=1}^{M}\sum_{j=1}^{k} a_{Mij}(m)\,R_{jh}(\iota - m) = R_{ih}(\iota) \quad (h = 1,2,\ldots,k;\ \iota = 1,2,\ldots,M) \tag{5b}$$

are used to calculate the coefficient $a_{Mij}(m)$.

Equation (5b) for each value of i ($i = 1,2,\ldots,k$) becomes $(M \times k)$-dimensional simultaneous equations. Thus, the larger the value of M and k, the longer it takes to calculate equation (5b). By combining Levinson–Durbin algorithm and FPE (final prediction error) procedure proposed by Akaike,[14] order M and the coefficients $a_{Mij}(m)$ can be computed precisely.

Considering the given data as $\{x_1(s\Delta t)\,x_2(s\Delta t)\,\ldots x_k(s\Delta t)\}$ where $(s = 1,2,\ldots,N)$ and Δt as the time interval of the data, the value of M and coefficients $a_{Mij}(m)$ can be computed by the following procedures:[14]

(i) *Removal of the mean value.* The mean value, $\bar{x}_i$, for $i = 1,2,\ldots,k$ must be computed first:

$$\bar{x}_i = \frac{1}{N}\sum_{s=1}^{N} x_i(s\Delta t) \tag{6}$$

Then, calculate

$$x_i(s) = x_i(s\Delta t) - \bar{x}_i \tag{7}$$

where $s = 1,2,\ldots,N$.

(ii) *Calculation of the estimated value of cross-correlation function.* The true autocorrelation or cross-correlation, $R_{ij}(\iota)$, in equation (5a) is estimated as follows:

$$R_{ij}(\iota) \approx C_{ij}(\iota) = \frac{1}{N}\sum_{s=1}^{N-\iota} x_i(s+\iota)\,x_j(s) \tag{8}$$

where $i,j = 1,2,\ldots,k$ and $\iota = 0,1,2,\ldots,L$.

(iii) *Identification of the elements of coefficient matrix* $[A_0(m)]$. Assume that the coefficient matrix $[A_0(m)] = [0]$ for $m = 1,2,\ldots,L$.

(iv) *Calculation of coefficient* $a_{Mij}(m)$. Using the Levinson–Durbin algorithm, element $a_{Mij}(m)$ of $[A_M(m)]$ $(m = 1,2,\ldots,M)$ and $[d_M]$ are calculated for $M = 0,1,2,\ldots,L$.

$$[d_M] = [C(0)] - \sum_{m=1}^{M} [A_M(m)]\,[C(m)]^{\mathrm{T}} \tag{9}$$

(v) *Calculation of MFPE.* MFPE which indicates the estimated error is calculated step by step at $M = 0,1,2,\ldots,L$ using the following equation:

$$\mathrm{MFPE}(M) = \left(1 + \frac{Mk+1}{N}\right)^{k}\left(1 - \frac{Mk+1}{N}\right)^{-k} |[d_M]| \tag{10}$$

(vi) *Calculation of the final values of M and* $a_{Mij}(m)$. In this procedure, the M value which gives the minimum value of MFPE will be used as the order number M of the AR model, and the coefficient $a_{Mij}(m)$ corresponding to the M value is also considered.

Calculation of wave propagation property

Considering the coefficient $a_{Mij}(m)$ obtained, the corresponding time series at one observation point can be computed by introducing a time series like a shape of a unit impulse at a particular time at the other

observation point. The method which is considered the basis of SIORM is introduced in this study. For simplicity, the following equations are derived in case $k = 2$, i.e. two time series.

The impulse response obtained in this study using the method in which SIORM is based differs from the usual impulse response of the autoregression model. In the usual model, the noise (external force) in equation (1) or equation (4) [for example $\varepsilon_1(s)$ where $s = 1, 2, \ldots$] included in $\{X(s)\} = \{x_1(s)\, x_2(s)\}^{\mathrm{T}}$ is a pulse state. In this study, the time series, $x_1(s)$ (for $s = 1, 2, \ldots$), is like a shape of a unit impulse at a particular time. Thus in this study, the noise (external force) $\{U(s)\} = \{\varepsilon_1(s)\, \varepsilon_2(s)\}^{\mathrm{T}}$ (for $s = 1, 2, \ldots$) is neither a pulse nor a white noise.

SIORM formulation

A unit impulse is set at a particular time at an observation point and the wave shape is not necessarily zero at any other time. The sum of squares and the sum of the square of the difference between two successive values of the wave shape are minimized in order to obtain a smooth response function. Considering these conditions and using equation (1) or equation (4), the time series at the other observation point can be computed.

Two time series $[x_1(s), x_2(s)$ where $s = 1, 2, \ldots, N']$ which express the wave propagation are formed by using equation (1) or equation (4). Considering noise $\varepsilon_1(s)$ (where $s = 1, 2, \ldots, N'$) and added to $x_1(s)$, an impulse wave shape is derived. If noise $\varepsilon_2(s)$ (where $s = 1, 2, \ldots, N'$) is not added to $x_2(s)$ the following equations are formulated:

$$
\begin{bmatrix}
1 & & & & & & : & 0 & & & & & \\
-a_{11}(1) & 1 & & & & & : & -a_{12}(1) & 0 & & & & \\
-a_{11}(2) & -a_{11}(1) & 1 & & \mathbf{0} & & : & -a_{12}(2) & -a_{12}(1) & 0 & & \mathbf{0} & \\
-a_{11}(3) & -a_{11}(2) & -a_{11}(1) & 1 & & & : & -a_{12}(3) & -a_{12}(2) & -a_{12}(1) & 0 & & \\
\vdots & & & & \ddots & & : & \vdots & & & & \ddots & \\
-a_{11}(M) & & & & & \ddots & : & -a_{12}(M) & & & & & \ddots \\
 & \ddots & & & & & : & & \ddots & & & & \\
\mathbf{0} & & -a_{11}(M) \cdots & -a_{11}(3) & -a_{11}(2) & -a_{11}(1)\ 1 & : & \mathbf{0} & & -a_{12}(M) \cdots & -a_{12}(3) & -a_{12}(2) & -a_{12}(1)\ 0 \\
\cdots & \cdots & \cdots & \cdots & \cdots & \cdots & : & \cdots & \cdots & \cdots & \cdots & \cdots & \cdots \\
0 & & & & & & : & 1 & & & & & \\
-a_{21}(1) & 0 & & & & & : & -a_{22}(1) & 1 & & & & \\
-a_{21}(2) & -a_{21}(1) & 0 & & \mathbf{0} & & : & -a_{22}(2) & -a_{22}(1) & 1 & & \mathbf{0} & \\
-a_{21}(3) & -a_{21}(2) & -a_{21}(1) & 0 & & & : & -a_{22}(3) & -a_{22}(2) & -a_{22}(1) & 1 & & \\
\vdots & & & & \ddots & & : & \vdots & & & & \ddots & \\
-a_{21}(M) & & & & & \ddots & : & -a_{22}(M) & & & & & \ddots \\
 & \ddots & & & & & : & & \ddots & & & & \\
\mathbf{0} & & -a_{21}(M) \cdots & -a_{21}(3) & -a_{21}(2) & -a_{21}(1)\ 0 & : & \mathbf{0} & & -a_{22}(M) \cdots & -a_{22}(3) & -a_{22}(2) & -a_{22}(1)\ 1
\end{bmatrix}
\times
\begin{Bmatrix}
x_1(1) \\ x_1(2) \\ x_1(3) \\ \vdots \\ x_1(N') \\ \cdots\cdots \\ x_2(1) \\ x_2(2) \\ x_2(3) \\ \vdots \\ x_2(N')
\end{Bmatrix}
=
\begin{Bmatrix}
\varepsilon_1(1) \\ \varepsilon_1(2) \\ \varepsilon_1(3) \\ \vdots \\ \varepsilon_1(N') \\ \cdots\cdots \\ 0 \\ 0 \\ 0 \\ \vdots \\ 0
\end{Bmatrix}
\tag{11}
$$

In order to express equation (11) in a compact form, let

$$\{Y_1\} = \{x_1(1)\, x_1(2)\, x_1(3)\, \ldots\, x_1(N')\}^{\mathrm{T}} \tag{12a}$$

$$\{Y_2\} = \{x_2(1)\, x_2(2)\, x_2(3)\, \ldots\, x_2(N')\}^{\mathrm{T}} \tag{12b}$$

$$\{V\} = \{\varepsilon_1(1)\, \varepsilon_1(2)\, \varepsilon_1(3)\, \ldots\, \varepsilon_1(N')\}^{\mathrm{T}} \tag{12c}$$

Then equation (11) can be written as

$$\begin{bmatrix} [B_{11}] & [B_{12}] \\ [B_{21}] & [B_{22}] \end{bmatrix} \begin{Bmatrix} \{Y_1\} \\ \{Y_2\} \end{Bmatrix} = \begin{Bmatrix} \{V\} \\ \{0\} \end{Bmatrix} \tag{13}$$

Simplifying equation (13), two equations are obtained:

$$[[B_{11}]\, [B_{12}]] \begin{Bmatrix} \{Y_1\} \\ \{Y_2\} \end{Bmatrix} = \{V\} \tag{14}$$

$$[[B_{21}]\, [B_{22}]] \begin{Bmatrix} \{Y_1\} \\ \{Y_2\} \end{Bmatrix} = \{0\} \tag{15}$$

Since $\{V\}$ in equation (14) is unknown, equation (15) is used to solve $\{Y_1\}$ and $\{Y_2\}$.

Simplifying equation (15),

$$[B_{21}]\, \{Y_1\} + [B_{22}]\, \{Y_2\} = \{0\} \tag{16}$$

Considering a rigorous unit impulse at $s = s_0$ for $x_1(s)$, the equation below is obtained:

$$\{Y_1\} = \{0 \ldots \underset{\hat{s}_0}{0\, 1\, 0} \ldots 0\}^{\mathrm{T}} \tag{17}$$

Then considering equations (16) and (17), $\{Y_2\}$ can be obtained using the equation

$$\{Y_2\} = -\,[B_{22}]^{-1}\, [B_{21}]\, \{Y_1\} \tag{18}$$

However, in some cases, the result of the computation of time series using equation (18) becomes unstable and divergent (an example is shown later in Figure 4(f)A). Therefore, a unit impulse is set at a particular time at an observation point and the wave shape function is not necessarily zero at any other time. Then, instead of equation (17) the following equation is used:

$$x_1(s_0) = 1 \tag{19}$$

This can be expressed also in the form

$$\{0 \ldots \underset{\hat{s}_0}{0\, 1\, 0} \ldots 0\} \begin{Bmatrix} \{Y_1\} \\ \{Y_2\} \end{Bmatrix} = 1 \tag{20}$$

Using equations (15) and (20), an equation is obtained:

$$\begin{bmatrix} [B_{21}] & & & [B_{22}] \\ 0 & \ldots\ \underset{\hat{s}_0}{0\, 1\, 0}\ \ldots & & 0 \end{bmatrix} \begin{Bmatrix} \{Y_1\} \\ \{Y_2\} \end{Bmatrix} = \begin{Bmatrix} \{0\} \\ 1 \end{Bmatrix} \tag{21}$$

In order to express equation (21) in a compact form, let

$$[G] = \begin{bmatrix} [B_{21}] & & & & [B_{22}] \\ 0 & \dots & 0\ 1\ 0 & \dots & 0 \end{bmatrix} \qquad \hat{s}_0 \tag{22}$$

$$\{d\} = \begin{Bmatrix} \{0\} \\ 1 \end{Bmatrix} \tag{23}$$

$$\{Y\} = \begin{Bmatrix} \{Y_1\} \\ \{Y_2\} \end{Bmatrix} = \{x_1(1)\, x_1(2)\, \dots\, x_1(N') \vdots\, x_2(1)\, x_2(2)\, \dots\, x_2(N')\}^{\mathrm{T}} \tag{24}$$

Then equation (21) can be written as

$$[G]\{Y\} = \{d\} \tag{25}$$

The equation which should be minimized in order to obtain a smooth response function is written below:

$$Q' = \sum_{i=1}^{2} \left[\sum_{s=1}^{N'} x_i(s)^2 + W \sum_{s=1}^{N'-1} \{x_i(s+1) - x_i(s)\}^2 \right] \tag{26}$$

where W is the weight value. In order to minimize equation (26), the method of Lagrange multiplier[19] should be applied. By using the method of Lagrange multiplier and also considering equation (25), $\{Y\}$ can be obtained as

$$\{Y\} = [L]^{-1}[G]^{\mathrm{T}}([G][L]^{-1}[G]^{\mathrm{T}})^{-1}\{d\} \tag{27}$$

The additional matrix $[L]$ in equation (27) is defined as

$$[L] = \left[\begin{array}{ccccc:ccccc}
W'' & -1 & & & \mathbf{0} & & & & & \\
-1 & W' & -1 & & & & & & & \\
 & -1 & W' & & -1 & & & \mathbf{0} & & \\
 & & \ddots & \ddots & & & & & & \\
\mathbf{0} & & & W' & -1 & & & & & \\
 & & & -1 & W'' & & & & & \\
\hdashline
 & & & & & W'' & -1 & & & \\
 & & & & & -1 & W' & \ddots & & \mathbf{0} \\
 & & & \mathbf{0} & & & \ddots & \ddots & & \\
 & & & & & & -1 & W' & -1 & \\
 & & & & & & & -1 & W' & -1 \\
 & & & & & \mathbf{0} & & & -1 & W''
\end{array}\right] \tag{28}$$

where $W' = (1/W) + 2$ and $W'' = (1/W) + 1$.

VERIFICATION OF SIORM ACCURACY

In order to check for the accuracy of the method presented in this paper, data which include two types of waves have been considered. In each type of wave, SIORM has been applied and the results are compared with the results using the peak of the cross-correlation function. The procedures followed in generating the ground acceleration time series, $x_2(s)$, for each type of wave are discussed in the following sections.

Random wave shape

The SIORM method needs two observed ground acceleration time series which are denoted as $x_1(s)$ and $x_2(s)$. For this first checking, a random wave shape whose period is comparatively long is considered as $x_1(s)$ which is shown in Figure 1. In generating different variations of $x_2(s)$, the following cases are considered:

Case 1: $x_2(s) = x_1(s - \tau)$.

Case 2: $x_2(s) = x_1(s - \tau) + x_1(s - 2\tau)$.

Case 3: $x_2(s) = x_1(s - \tau) + x_1(s - 2\tau) + x_1(s - 3\tau)$.

Case 4: $x_2(s) = x_1(s - \tau) + x_1(s - 2\tau) + x_1(s - 3\tau) + x_1(s - 4\tau)$.

The different variations of $x_2(s)$ obtained are also shown in Figure 1. The number of elements N considered in each data $x_1(s)$ and $x_2(s)$ is 200 while $\tau = 5$ steps. After generating $x_2(s)$, SIORM is applied and its results are compared with the results obtained using the peak of the cross-correlation function. The results of cross-correlation function of $x_1(s)$ and $x_2(s)$ and SIORM by using equation (18) are shown in Figures 2 and 3, respectively.

Most of the results obtained using the peak of the cross-correlation function of $x_1(s)$ and $x_2(s)$ did not show any consistency for the different variations of $x_2(s)$. In case 1, the result of the cross-correlation function clearly shows that $x_2(s)$ is τ step lag from $x_1(s)$. However, the peak of the cross-correlation function for the other cases which are shown in Figure 2 did not coincide with the way the different cases of $x_2(s)$ are obtained. These results show that not only the different variation used in obtaining $x_2(s)$ but also the shape of the autocorrelation function influenced the results.

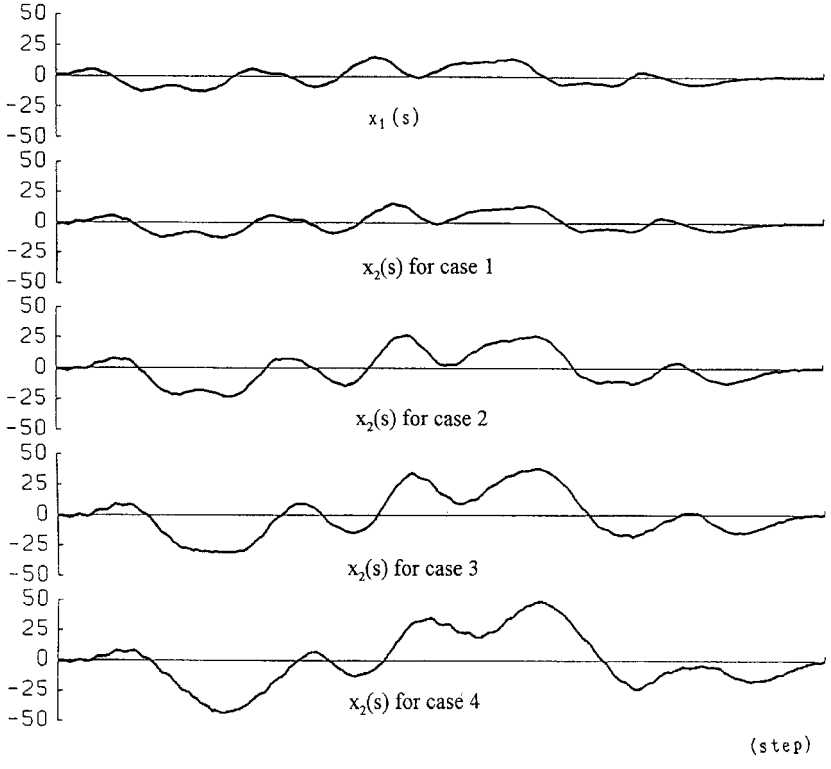

Figure 1. Random wave shape

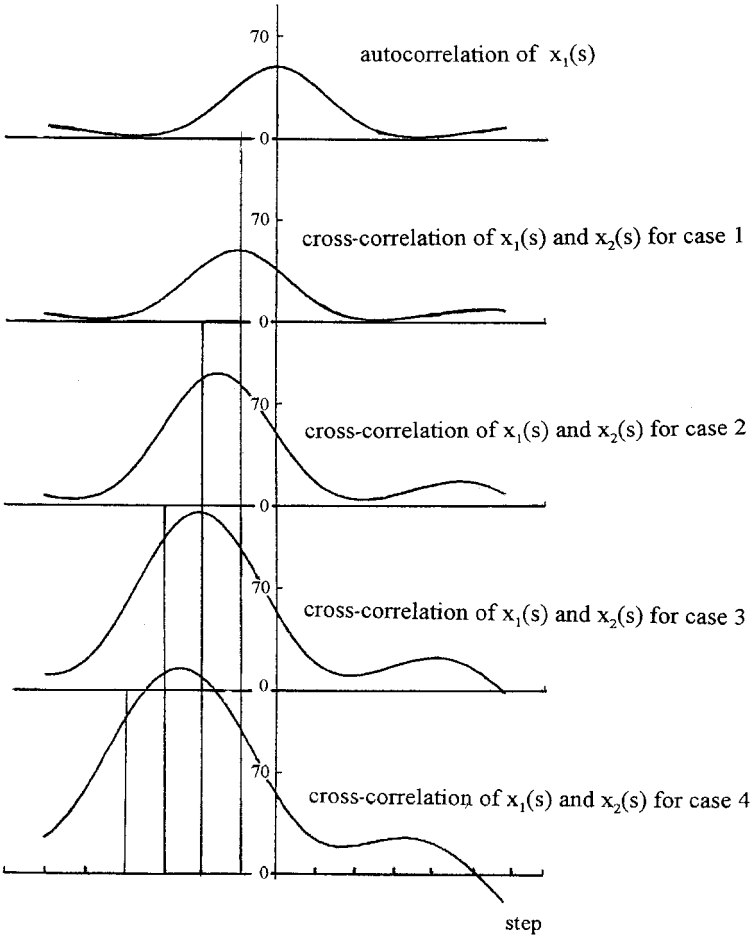

Figure 2. Correlation functions of $x_1(s)$ and $x_2(s)$

The results obtained using SIORM which are shown in Figure 3 show a clearer peak compared with the peak of the cross-correlation function. The result for case 1 shows a single peak whose amplitude is almost one and which is τ steps from the location of the unit impulse considered at $x_1(s)$. For cases 2, 3 and 4, the number and location of peaks coincide with the way how $x_2(s)$ are obtained in cases 2, 3 and 4. In case 2, the peaks are located at τ and 2τ, case 3 at τ, 2τ and 3τ and in case 4 at τ, 2τ, 3τ and 4τ lag times.

Effect of noise

In the first type of wave noise is not considered and the obtained results verified the accuracy of SIORM. The second type of wave that will be considered is a wave with noise. Figure 4 shows $x_1(s)$, $x_2(s)$ and SIORM (equation (18)) results. Figure 4(a) shows a generated wave considered as $x_1(s)$ while Figure 4(b) shows sine waves with different amplitudes and frequencies and considered as the noise. Noise A in Figure 4(b) does not look like a sine wave because the sampling rate is not small enough in comparison with the period of the sine wave. Figure 4(c) shows $x_2(s)$ without noise and obtained by considering $\tau = 10$ step lag in $x_1(s)$. Figure 4(d) shows the different variations of $x_2(s)$ which are obtained by combining the $x_2(s)$ in Figure 4(c) and the different types of noise in Figure 4(b).

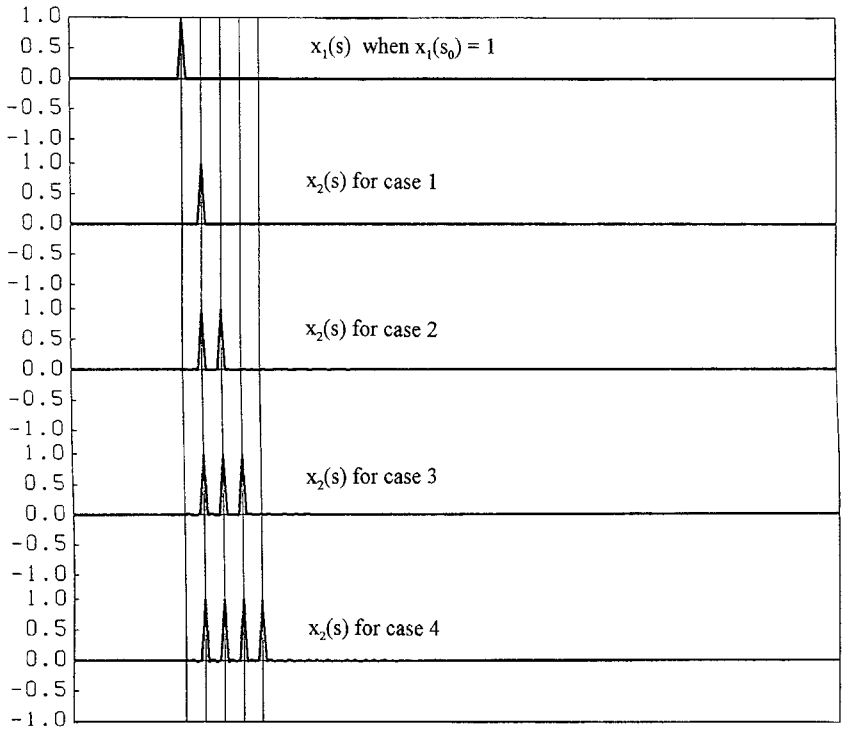

Figure 3. SIORM result for checking of random wave shape

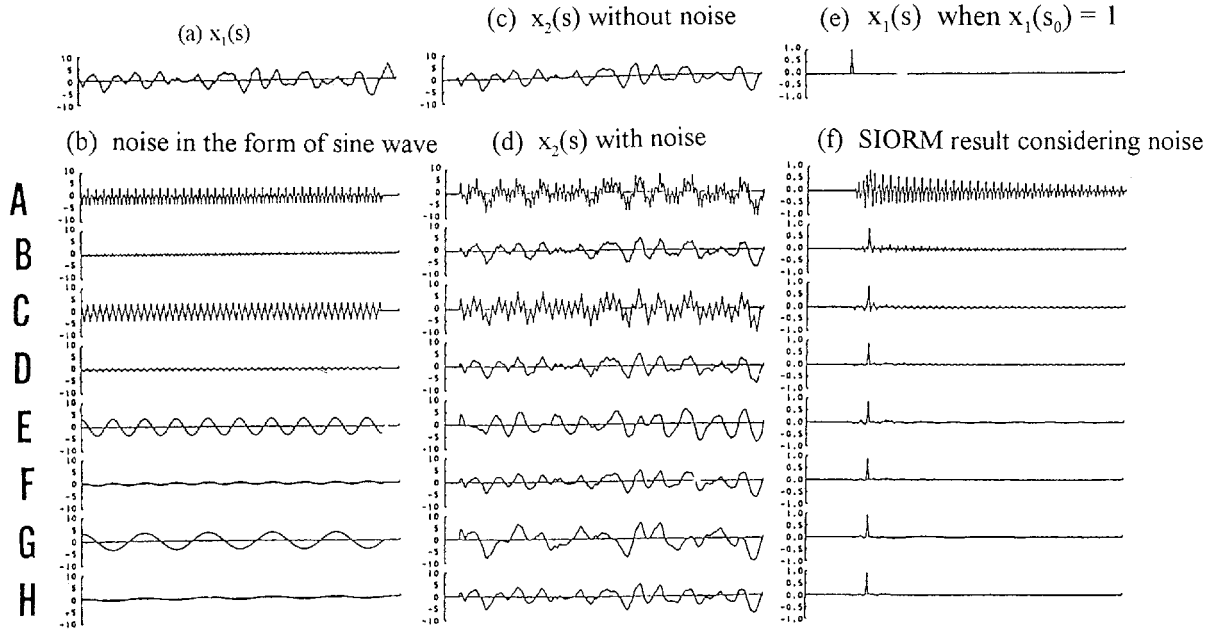

Figure 4. $x_1(s)$, $x_2(s)$ and result of SIORM when noise is considered

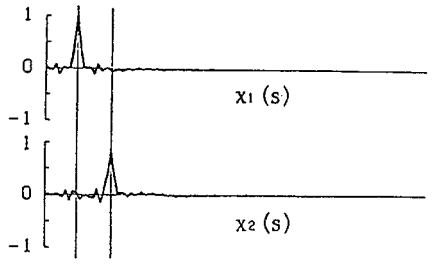

Figure 5. Result minimizing the effect of noise

The result using SIORM for different $x_2(s)$ with noise considered are shown in Figure 4(f). The results in the computation considering B to H type of noise show a clear peak which is located at $\tau = 10$ steps. However, in the case of A type of noise which is a short period sine wave with large amplitude, the obtained result of SIORM is complex and shows a number of peaks not only located at $\tau = 10$ steps. These results show that high-frequency noise of large amplitude may cause more effect on the accuracy of the method. In order to minimize the effect of noise on the result of SIORM, equation (27) is used instead of equation (18), and the results are shown in Figure 5. From the results shown, the effect of noise had been minimized and obtained result is similar to the expected theoretical result.

The results of the evaluation of the SIORM on the two wave types suggest its accuracy and superiority over the peak of the cross-correlation function in generating a simpler and accurate result. For this reason, SIORM can be used in wave propagation analysis.

APPLICATION TO ACTUAL EARTHQUAKE RECORDS

In order to evaluate the method presented in this paper, SIORM is applied to actual ground acceleration time history records.[20] A total of four sets of strong ground motion records taken at Minamisuna and Etchujima sites in Japan are used in the actual application of SIORM. All the components that are studied are listed in Table I.

Minamisuna observation site

There are 7 observation points in this particular site. However, in the time history record dated 8 August, 1983, G7 (observation point at elevation $-28{\cdot}2$ m) did not have any time history record. Figure 6 shows the geological and geophysical characteristics and the observation points of the array. Since the SIORM is applied to a non-stationary time series, moving-window approach is adopted.[16] In this approach, segments of the record which are short enough to be considered approximately stationary but still long enough to contain sufficient data points for stable estimation are analysed separately. In most of the computation for the Minamisuna site, a segment of 10 s is found to provide a satisfactory window. In considering the windows corresponding to $x_1(s)$ and $x_2(s)$, a lag time, τ, is considered. This lag time, τ, means that $x_2(s)$ is actually $x_2(s-\tau)$ in the original time history record. This also means that in plotting the response obtained using SIORM, $x_2(s)$, at different observation points, $x_2(s-\tau)$ should be used instead of $x_2(s)$. In the application of SIORM at both Minamisuna and Etchujima sites, the value of lag time, τ, is equal to $0{\cdot}75$ s. The P-wave and S-wave portions of each record are analysed separately in order to determine the wave propagation properties on each particular portion of the record.

Using the SIORM, a unit impulse is considered at G1 and the response at different observation points are shown in Figures 7 and 8. In the application of SIORM at both Minamisuna and Etchujima sites, the weight

Table I. Aspects of the different ground acceleration records considered

Observation site	Date	Depth (km)	M	Epicentral distance (km)	PGA (gal)	Components
Minamisuna	1983.08.08	22	6·0	74	16	NS, EW
	1987.04.07	44	6·6	258	14	NS, EW
Etchujima	1983.08.08	22	6·0	72	32	NS, EW
	1987.12.17	58	6·7	71	87	NS, EW

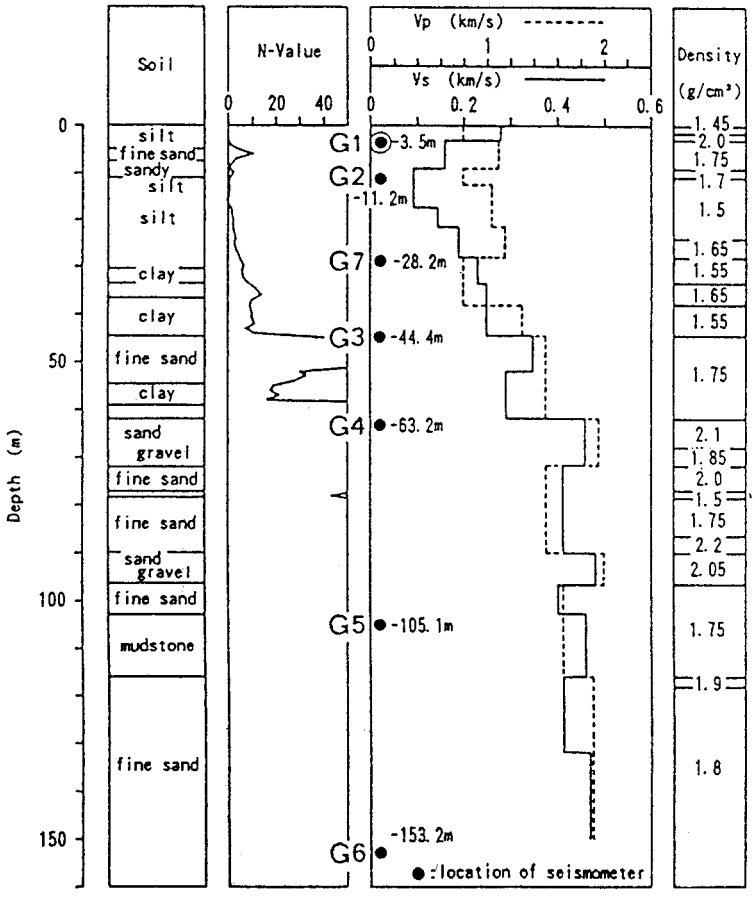

Figure 6. Geological and geophysical characteristics of Minamisuna site[20]

value, W, considered is 0·5. In order to validate the result, time arrivals of P-waves and S-waves are computed at different observation points based on geophysical and geological information and the results are also included in the said figures. The centre solid vertical line in Figures 7 and 8 denotes zero time. The inner two broken lines denote the time arrival of P-wave while the outer two broken lines denote the time arrival of S-wave. Each of the impulse response at different observation points show two relatively large peaks which are related to incident and reflected S-waves. In order to check the obtained peaks, the time order of the input

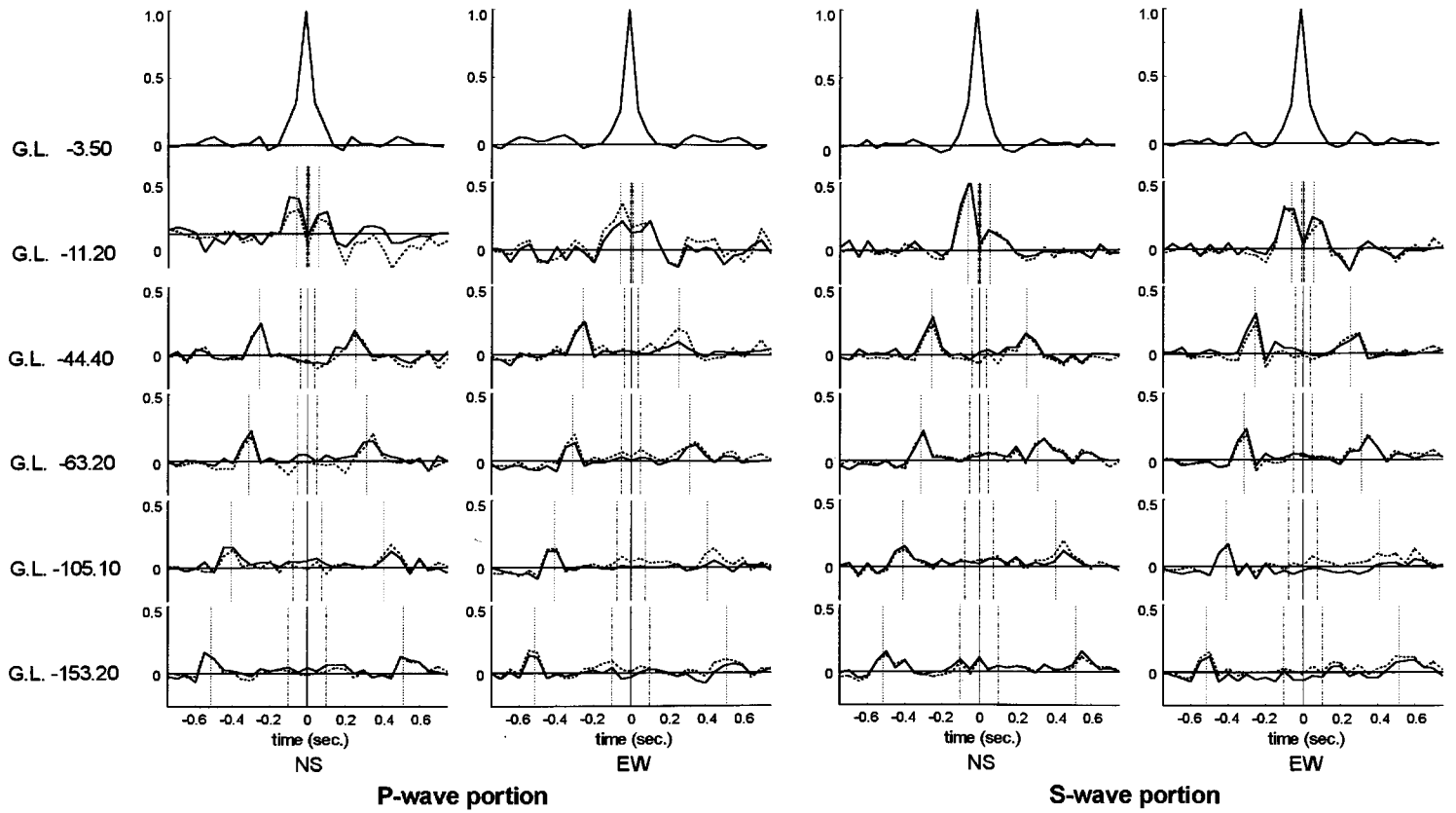

Figure 7. SIORM result for ground acceleration time history record dated 8 August 1983 at Minamisuna site

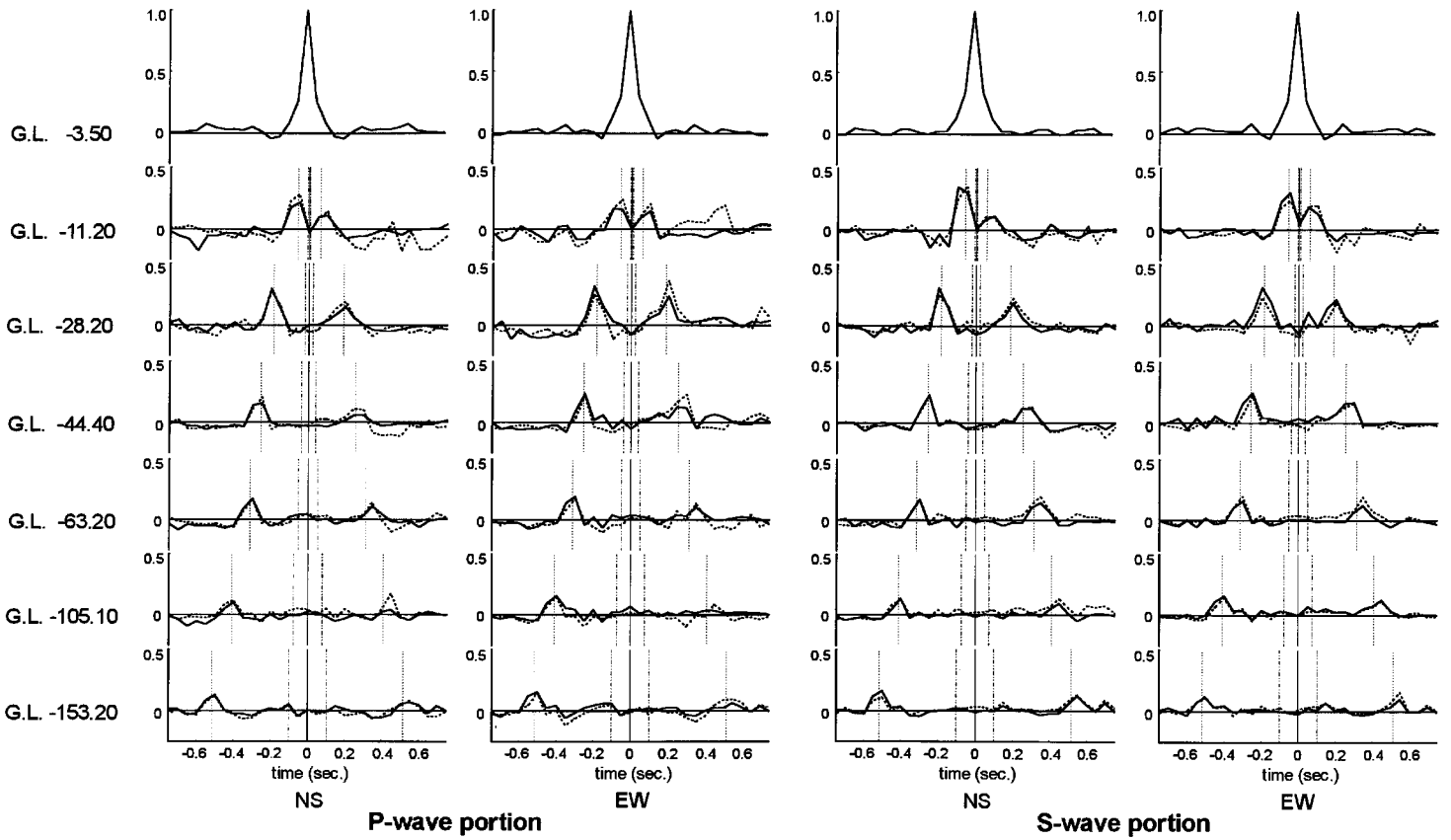

Figure 8. SIORM result for ground acceleration time history record dated 7 April 1987 at Minamisuna site

Table II. Soil profile and system layout for Etchujima observation site[20]

Depth (m)	Soil type	Soil density (g/cm^3)	P-velocity (km/s)	S-velocity (km/s)	Location of seismometer
0–4	Sandy silt	1·7	0·62	0·11	GL. − 1·0 m
4–11			0·94		
11–16	Clayey silt	1·6		0·13	
16–26			1·33		
26–33	Sandy silt	1·7		0·23	
33–37			0·93		
37–53	Sand and gravel	2		0·44	GL. − 40·0 m
53–70					
70–75	Fine-grained sand	1·85	1·75	0·3	
75–83				0.46	
83–100	Mud	1·9			GL. − 100·0 m

waves has been reversed and SIORM is applied considering that in equations (1) and (4) only positive values of m are used. The broken line in Figures 7 and 8 shows the result considering the reverse order of time. Based on the checking performed considering the geological data and geophysical data and also reversing the time order, SIORM showed a good result.

Etchujima observation site

The geological and geophysical characteristics of Etchujima observation site are summarized in Table II. The soil profile of this site consists of six layers. The different observation points at this site are located at 1, 40 and 100 m depths.

For the ground motion record dated 8 August 1983, a 10·2 s window is used for both P-wave and S-wave portions. In the other record dated 17 December 1987, a 10 s window is used. The results of SIORM on each record are shown in Figures 9 and 10. Two clear peaks representing the incident and reflected waves are consistent with the result using the geophysical data on the site. However, it can be noted that the arrival times of both incident and reflected waves in the NS and EW components are roughly equal to the theoretical result of S-wave travelling orthogonal to the ground surface for both P-wave and S-wave portions.

The results of SIORM application to the ground acceleration records taken from both Minamisuna and Etchujima sites show interesting findings about the wave propagation properties. One of the findings is that both NS and EW (horizontal) components travel in the S-wave velocity as shown in the results in Figures 7–10. The results also show that even in the P-wave portion of the ground acceleration record the horizontal component travels in S-wave velocity instead of P-wave velocity. SIORM result also illustrates the relationship between the incident and reflected waves in which the amplitude of the incident wave is greater than that of the reflected wave. This finding is consistent with the common knowledge that the amplitude of the incident wave is greater than that of the reflected wave.

CONCLUSIONS

In this paper, a Simplified Input Output Relation Method (SIORM) using AR model for wave propagation analysis is presented. Using the AR model, a method has been developed to establish the basis for the

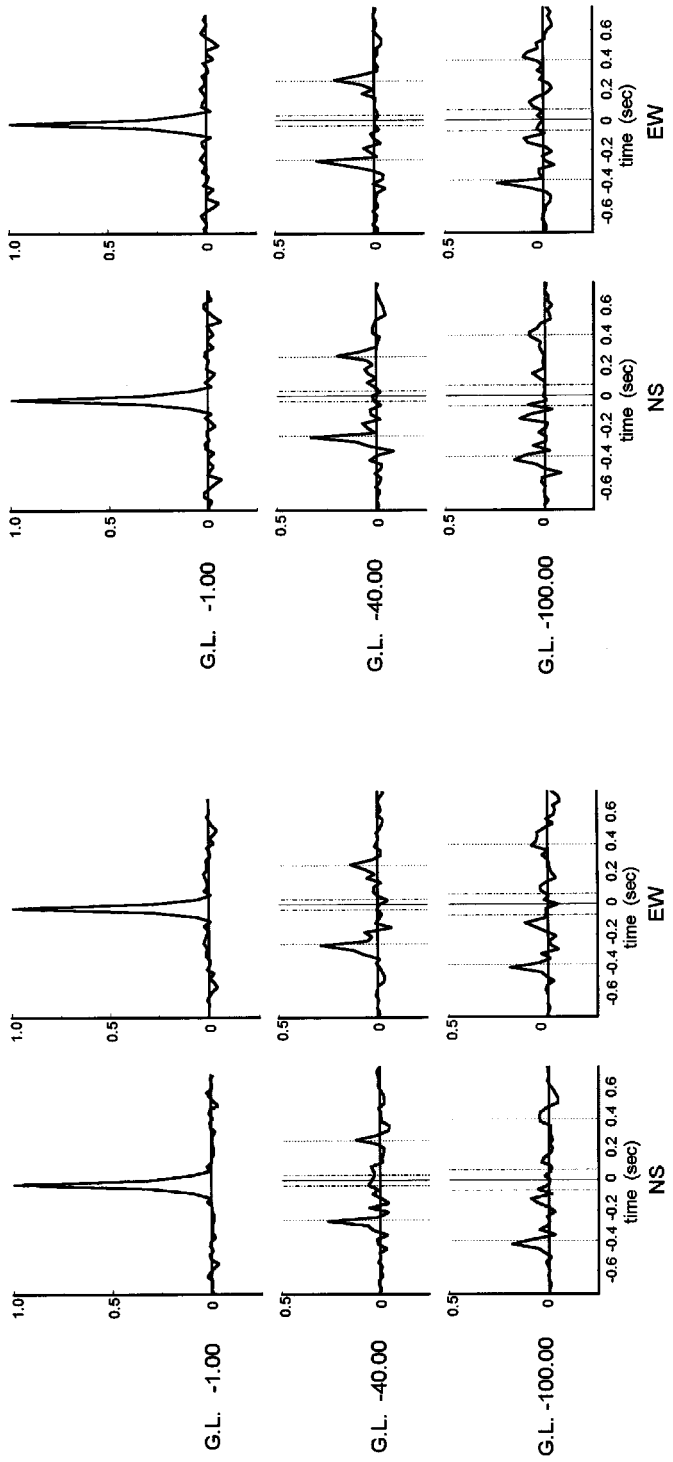

Figure 9. SIORM result for ground acceleration time history record dated 8 August 1983 at Etchujima site

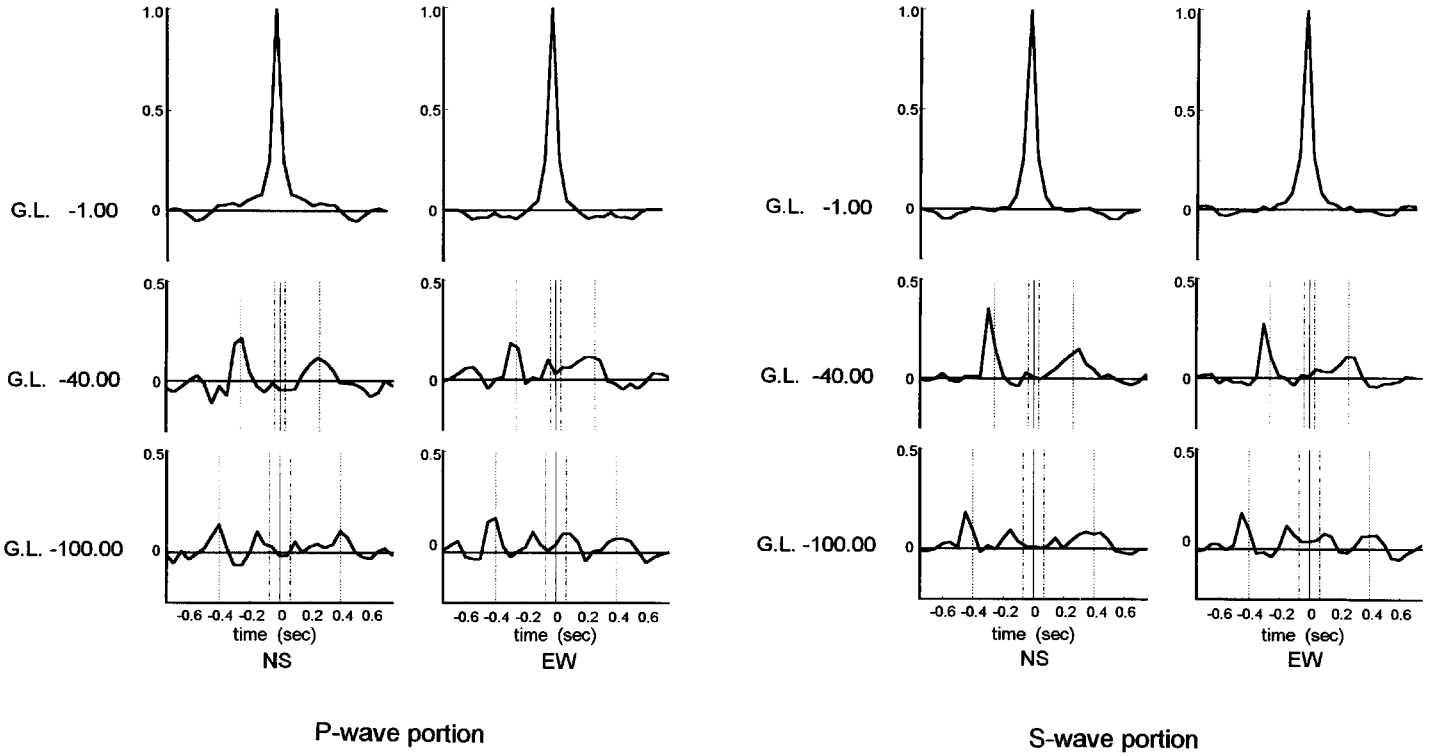

Figure 10. SIORM result for ground acceleration time history record dated 17 December 1987 at Etchujima site

formulation of the SIORM. This method is evaluated as to the extent to which the effect of noise is minimized and the time arrival and amplitude of the wave approximate the theoretical results.

Application of SIORM to actual ground acceleration time history records of Minamisuna and Etchujima sites revealed a very clear arrival time of incident S-wave and reflected S-wave from the surface. The result showed consistency with the theoretical time arrival of the S-wave when geological and geophysical data are used. SIORM result also illustrates the relationship between the incident and the reflected waves in which the amplitude of the incident wave is greater than that of the reflected wave. This finding is consistent with the common knowledge that the amplitude of the incident wave is greater than that of the reflected wave. The study suggests that SIORM can be used to investigate the time arrival of the incident and reflected waves using actual ground acceleration time history records. Moreover, the amplitude of the incident and reflected wave at each observation point can be examined.

ACKNOWLEDGMENTS

We would like to acknowledge the generosity of the Association for Earthquake Disaster Prevention of Japan for providing the strong motion array record database used in the application of the method presented in this study. We would like also to express our sincerest gratitude to Takenaka Corporation Technical Research Laboratory and Shimizu Corporation which are operating and maintaining the Minamisuna and Etchujima vertical arrays.

REFERENCES

1. E. Shima *et al*., 'Underground structure of Tokyo metropolitan area', *Bull. earthquake res. inst. univ. Tokyo* **51**, 1–11 (1976) (in Japanese).
2. B. A. Bolt, Y. B. Tsai, K. Yeh and M. K. Hsu, 'Earthquake strong motions recorded by a large near-source array of digital seismographs', *Earthquake engng. struct. dyn.* **10**, 561–573 (1982).
3. C. H. Loh, J. Penzien and Y. B. Tsai, 'Engineering analyses of SMART 1 array accelerograms', *Earthquake engng struct. dyn.* **10**, 575–591 (1982).
4. E. Kausel and A. Pais, 'Stochastic deconvolution of earthquake motions', *J. eng. mech. ASCE*, **113**, 266–277 (1987).
5. K. Kanai, T. Tanaka and S. Yoshizawa, 'Comparative studies of earthquake motions on the ground and underground (multiple reflection problem)', *Bull. earthquake res. inst. univ. Tokyo* **37**, 53–87 (1959).
6. H. B. Seed and I. M. Idriss, 'Influence of soil conditions on ground motions during earthquakes', *J. soil mech. fndns. div. ASCE* **95**, 99–137 (1969).
7. S. Okamoto, *Introduction to Earthquake Engineering*, 2nd edn, University of Tokyo Press, Tokyo, 1984.
8. E. Safak, 'Problems with using spectral ratios to estimate site amplification', *Proc. 4ICSZ*, 1991, pp. 277–284.
9. M. R. Ghayamghamian and H. Kawakami, 'On the characteristics of non-linear soil response and dynamic soil properties using vertical array data in Japan', *Earthquake engng. struct. dyn.* **25**, 857–870 (1996).
10. C. Tamura, S. Okamoto and H. Kawakami, 'Earthquake ground motion at rocky ground interspersed with thin soft layers', *Bull. earthquake resistant struct. res. center, Univ. Tokyo* (10), 11–29 (1976).
11. S. Kurita, M. Izumi, S. Iizuka, T. Sato and T. Aiba, 'Statistical characteristics of seismic wave propagation in soil with vertical instruments array', *Proc. 9th world conf. on earthquake eng*., Tokyo and Kyoto, Japan, Vol. II, 1988.
12. M. Horike, 'Inversion of phase velocity of long-period microtremors to the S-wave velocity structure down to the basement in urbanized areas', *J. phys. earth* **33**, 59–96 (1985).
13. J. Capon, 'High-resolution frequency-wavenumber spectrum analysis', *Proc. IEEE* **57**, 1408–1418 (1969).
14. H. Akaike, *Statistical Analysis and Control of Dynamic System*, Science Inc., Tokyo, 1972 (in Japanese).
15. C. W. J. Granger and P. Newbold, *Forecasting Economic Time Series*, Academic Press, New York, 1977.
16. M. K. Chang, J. W. Kwiatkowski, R. F. Nau, R. M. Oliver and K. S. Pister, 'ARMA models for earthquake ground motions', *Earthquake engng. struct. dyn.* **10**, 651–662 (1982).
17. S. Makridakis, S. C. Wheelwright and V. E. McGee, *Forecasting*: *Methods and Applications*, 2nd edn, Wiley, New York, 1983.
18. M. Hoshiya and H. Kurita, 'Autoregressive model of multiple points earthquake ground motions', *Proc. 9th world conf. on earthquake eng*., Tokyo and Kyoto, Japan, Vol. II, 1988.
19. J. F. Claerbout, *Fundamentals of Geophysical Data Processing*, Blackwell Scientific Publications, 1985.
20. Database Advisory Committee and Working Sub-committee, *Strong Motion Array Record Database-Data Manual*, Association for Earthquake Disaster Prevention, Vol. A01, July 1992.

